Conference on Modelling Fluid Flow (CMFF'25)
The 19th International Conference on Fluid Flow Technologies
Budapest, Hungary, August 26-August 29, 2025

DEFINITION AND COMPUTATION OF A FLUTTER SAFETY MARGIN FOR QUADCOPTERS BY CHAINING TOGETHER MULTIPLE 2-DOF AEROELASTIC MODELS

Dávid András HORVÁTH[1], János LELKES[2], Balázs FARKAS[3], Tamás KALMÁR-NAGY[4]

[1] Corresponding Author. Department of Fluid Mechanics, Faculty of Mechanical Engineering, Budapest University of Technology and Economics. Bertalan Lajos u. 4 - 6, H-1111 Budapest, Hungary. E-mail: horvathd1@edu.bme.hu
[2] Robert Bosch Kft. E-mail: janos.lelkes@hu.bosch.com
[3] Department of Fluid Mechanics, Faculty of Mechanical Engineering, Budapest University of Technology and Economics. E-mail: farkas.balazs@gpk.bme.hu
[4] Department of Fluid Mechanics, Faculty of Mechanical Engineering, Budapest University of Technology and Economics. E-mail: kalmar.nagy.tamas@gpk.bme.hu

ABSTRACT

When thin, flexible structures, such as the rotors of a quadcopter, are subjected to airflow, aeroelastic phenomena can occur due to the interaction of elastic, inertial, and aerodynamic forces. Due to these phenomena, the flexible structures lose their stability at a critical flow velocity. Flutter is an aeroelastic instability that leads to dynamic stability loss. In this paper, we examine the flutter of the rotor blades during the forward flight of the quadcopter. In this regime, the relative wind experienced by the rotor blades changes periodically. This results in parametric excitation, which can lead to a reduced critical velocity compared to the case without parametric excitation. To consider that the relative wind changes along the radius of the rotor, we construct a three-dimensional reduced-order model by chaining multiple two-degree-of-freedom aeroelastic models. The aerodynamic forces acting on the two-degree-of-freedom models are computed using a quasi-steady aerodynamic model.

We apply the reduced-order model to compute the stability chart of a real quadcopter. To achieve this, we perform simple measurements on the rotor to obtain the geometric parameters, the stiffness, and the damping coefficients. We then compute the stability chart for the quadcopter by solving the equations of motion of the reduced-order model numerically. Using the computed stability chart, we can determine, for a given rotor speed and forward flight velocity, the minimal speed increase required for the rotors of the quadcopter to lose their stability. We call this minimal speed increase the flutter safety margin. We gather velocity data during the flight of a quadcopter and compute the flutter safety margin during the flight.

Keywords: aeroelasticity, fluid-structure interaction, numerical stability analysis, parametric excitation, quadcopter

1. INTRODUCTION

Aeroelastic phenomena affect several types of slender elastic structures subjected to airflow, such as flexible wings, helicopter rotor blades, and wind turbines. Aeroelasticity studies the interactions between inertial, elastic, and aerodynamic forces on flexible structures that are exposed to airflow. The theory of aeroelasticity is extensively covered in the literature [1, 2, 3]. One dangerous aeroelastic instability is called flutter, which is a dynamic stability loss [4]. A famous example of flutter is the vibrations and structural failure of the Tacoma Narrows bridge [5, 6].

Airflow oscillations can cause parametric excitation in aeroelastic systems [7]. Parametric excitation differs from external forcing. The excitation source during parametric excitation is the time-varying modification of a system parameter. In the case of airflow oscillations, the parameters of the aerodynamic lift and moment are time-varying. The interaction of self- and parametric excitation can increase or decrease the critical wind velocity.

Typically, a two-degrees-of-freedom (2-DOF) reduced-order model is used to investigate flutter and compute the critical velocity [8]. However, one major disadvantage of this model is that it assumes a uniform velocity along the wing, while rotorcraft, such as drones, have a linear velocity distribution along the span of their wings. Thus, it is important to study a more complex reduced-order model to gain a better understanding of flutter safety for these aircraft.

This work investigates a three-dimensional reduced-order model subjected to periodically varying airflow to study flutter in flying drones. In Section 2, we introduce the mathematical model. In Section 3, we compute the stability charts. In Section 4, we introduce the flutter safety margin and compute it during the flight of the drone. In Section 5, we summarize the results.

2. MATHEMATICAL MODEL

In this section, we will describe the three-dimensional reduced-order aeroelastic model. The building block of this model is a two-degrees-of-freedom (2-DOF) aeroelastic model shown in Figure 1. The two degrees of freedom in the model are the pitching (α) and plunging (h) degrees of freedom.

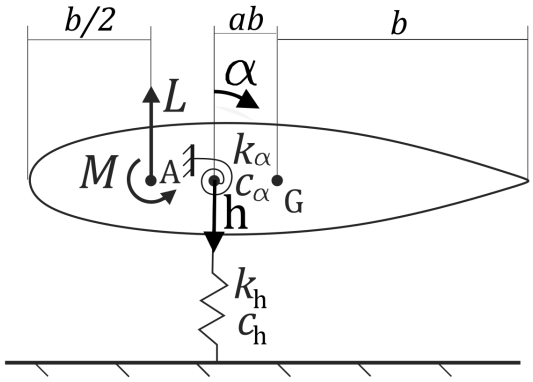

Figure 1. The 2-DOF aeroelastic model.

In this model, we assume that the center of gravity (denoted by G) is located in the middle of the wing. We denote the distance between the elastic axis and the center of gravity by ab and the semi-chord by b. The equations of motion of this model are [9].

$$\begin{aligned} m\ddot{h} + c_h\dot{h} + k_h h &= -L, \\ I_\alpha\ddot{\alpha} + c_\alpha\dot{\alpha} + k_\alpha\alpha &= M, \end{aligned} \tag{1}$$

where h and α describe the vertical (plunge) displacement (positive downwards) and angular (pitch) displacement (positive in the clockwise direction), respectively. The mass of the wing is m and I_α is the moment of inertia. The stiffness and damping coefficients for the plunge DOF are denoted by k_h and c_h, respectively. For the pitch DOF, these coefficients are denoted by k_α and c_α. L and M denote the aerodynamic lift and moment (together they will be called the aerodynamic forces). To compute the aerodynamic forces L and M, we apply the quasi-steady approximation of the Theodorsen lift function [10]. Thus,

$$\begin{aligned} L &= 2\pi\rho U^2 bS\left[\alpha + \frac{\dot{h}}{V} + b\left(\frac{1}{2} - a\right)\frac{\dot{\alpha}}{V}\right], \\ M &= 2\pi\rho U^2 b^2 S\left(a + \frac{1}{2}\right)\left[\alpha + \frac{\dot{h}}{V} + b\left(\frac{1}{2} - a\right)\frac{\dot{\alpha}}{V}\right], \end{aligned} \tag{2}$$

where S is the span of the wing, a is defined via Figure 1, ρ is the density of the air and V is the velocity of the air. One big disadvantage of this model is that it assumes a constant velocity distribution along the span of the wing. This assumption is not valid for rotorcraft, since in their case the velocity increases linearly from the hub to the tip of the wing.

We eliminate this disadvantage by chaining multiple two-degrees-of-freedom (2-DOF) models into a three-dimensional reduced-order model through a pair of springs. Each wing segment (i.e., a single 2-DOF model) has a pitch and plunge DOF, with the plunge DOF corresponding to the bending motion of the wing. These DOFs are coupled to those of the neighboring wing segments by springs. The construction is shown in Figure 2 for two wing segments.

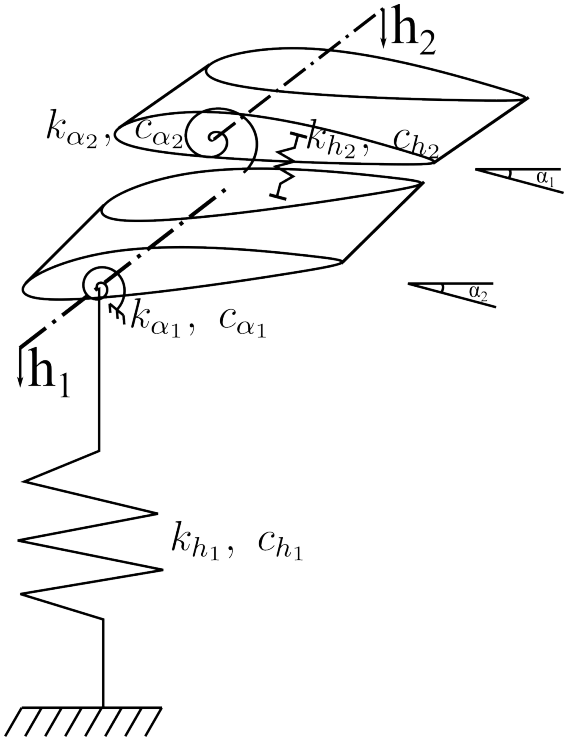

Figure 2. The three-dimensional reduced order model.

This construction consists of wing segments connected to each other by identical springs in a series configuration. The model is shown for two wing segments for simplicity, but it can be easily generalized for more segments. The equation of motion for this three-dimensional model is

$$\underline{\underline{M}}\ddot{x} + \underline{\underline{C}}\dot{x} + \underline{\underline{K}}x = \begin{bmatrix} L_1\left(\ddot{h}_1, \dot{h}_1, \alpha_1, \dot{\alpha}_1, \ddot{\alpha}_1\right) \\ M_1\left(\ddot{h}_1, \dot{h}_1, \alpha_1, \dot{\alpha}_1, \ddot{\alpha}_1\right) \\ L_2\left(\ddot{h}_2, \dot{h}_2, \alpha_2, \dot{\alpha}_2, \ddot{\alpha}_2\right) \\ M_2\left(\ddot{h}_2, \dot{h}_2, \alpha_2, \dot{\alpha}_2, \ddot{\alpha}_2\right) \end{bmatrix}, \tag{3}$$

where $L_i\left(\ddot{h}_i, \dot{h}_i, \alpha_i, \dot{\alpha}_i, \ddot{\alpha}_i\right), M_i\left(\ddot{h}_i, \dot{h}_i, \alpha_i, \dot{\alpha}_i, \ddot{\alpha}_i\right)$ are the lift and moment acting on the i-th wing segment, $\underline{\underline{M}}$, $\underline{\underline{C}}$, and $\underline{\underline{K}}$ are the mass, damping, and stiffness

matrices respectively, and $\underline{x} = [x_1, x_2, x_3, x_4]^T$ is the state vector. The four variables in the state vector are the two plunging displacements h_1, h_2 and the two pitching displacements α_1, α_2, i.e., $x_1 = h_1, x_2 = \alpha_1, x_3 = h_2, x_4 = \alpha_2$. The mass and stiffness matrices are derived using the principles of Lagrangian mechanics and are given by

$$\underline{\underline{M}} = \left[\frac{\partial^2 E_k}{\partial \dot{x}_i \partial \dot{x}_j}\right] \tag{4}$$

$$\underline{\underline{K}} = \left[\frac{\partial^2 U}{\partial x_i \partial x_j}\right], \tag{5}$$

where E_k is the kinetic energy and U is the potential energy of the system. We assume proportional damping, meaning that the damping matrix $\underline{\underline{C}}$ is a multiple of the stiffness matrix $\underline{\underline{K}}$, i.e.,

$$\underline{\underline{C}} = d\underline{\underline{K}}, \tag{6}$$

where d is a constant.

For the model we have taken the structural parameters from [9] but scaled them to match the dimensions and mass of our drone's propeller. The resulting parameters are shown in Table 1.

Parameter name	Parameter value
a	0
b	0.017 m
c_h	0.003 kg/s
c_α	0.006 kgm^2/s
Θ	0.00023 kgm^2
k_h	250 N/m
k_α	0.49 Nm/rad
m	0.008 kg
S	0.167 m
ρ	1.2 kg/m^3.

Table 1. Numerical values of the parameters in the three-dimensional reduced order model.

Now we will describe the parameters of the individual wing segments based on the parameters of the whole wing given in Table 1. The mass, moment of inertia, and span of the i-th wing segment are given by

$$m_i = \frac{m}{n}, \quad \Theta_i = \frac{\Theta}{n} \quad S_i = \frac{S}{n}, \tag{7}$$

where m_i, Θ_i, S_i are the mass, moment of inertia, and span of the i-th wing segment, respectively, and n is the number of wing segments. We approximate the stiffness coefficients by a linear function as

$$k_{\alpha_i} = k_\alpha(n - i + 1), \quad k_{h_i} = k_h(n - i + 1), \tag{8}$$

where k_{α_i}, k_{h_i} are the pitching and plunging stiffness coefficients of the i-th wing segment, respectively. It is not straightforward to determine the damping coefficient of the i-th wing segment. However, it was determined by [11] that the use of

$$c_{\alpha_i} = c_\alpha \sqrt{n}, \quad c_{h_i} = c_h \sqrt{n}, \tag{9}$$

leads to the fastest convergence of the critical velocity as a function of n. For this reason, we use these functions to obtain the damping coefficient of the i-th wing segment.

We will now compute the critical velocity of the model, which is the flow velocity at which the system loses its stability and flutter oscillations occur. First, we assume a constant velocity distribution along the wing. To compute the critical velocity, we determine the eigenvalues of the system's Jacobian for wind velocities starting from 0, increasing by 1 m/s up to 100 m/s. As the velocity increases, a pair of complex conjugate eigenvalues will cross the imaginary axis. The velocity at which this occurs is the critical velocity. The critical velocity as a function of the number of wing segments is shown in Figure 3.

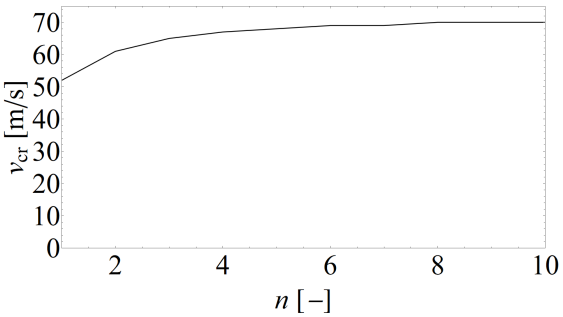

Figure 3. The critical velocity as a function of the number of wing segments assuming constant velocity distribution.

The critical velocity of the two-degrees-of-freedom (2-DOF) model is $52m/s$, which corresponds to $n = 1$. As the number of wing segments increases, the critical velocity also increases and converges to $70m/s$. Thus, the use of the three-dimensional model results in approximately 35% higher critical velocity, which confirms that this more complex model is indeed necessary to obtain accurate results even for fixed-wing aircraft.

Now we will investigate the critical velocity for drones, which have a linear velocity distribution along the wing, as follows:

$$v_i = v\frac{i}{n}, \tag{10}$$

where v_i is the wind velocity at the i-th wing segment. The critical velocity as a function of the number of wing segments is shown in Figure 4.

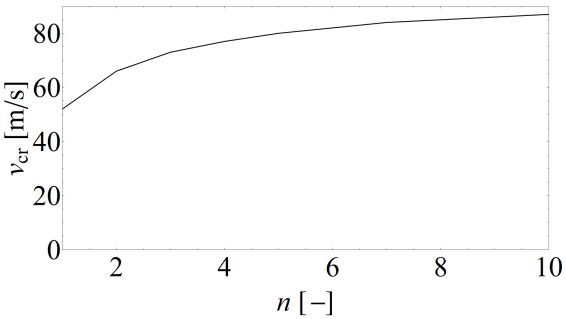

Figure 4. The critical velocity as a function of the number of wing segments assuming linear velocity distribution.

The critical velocity of the two-degrees-of-freedom (2-DOF) model is $52m/s$, which corresponds to $n = 1$. As the number of wing segments increases, the critical velocity also increases and converges to $82m/s$. Thus, the use of the three-dimensional model results in approximately 58% higher critical velocity. This critical velocity is also approximately 17% higher than in the previous case where we assumed constant velocity distribution along the wing.

3. STABILITY CHARTS

In this section, we will compute stability charts for the three-dimensional model, which show as a function of the rotor speed and the forward flight velocity, whether flutter occurs, i.e., the stability of the system.

As a first step, we need to compute the time-varying relative wind velocity experienced by the rotor blade as a function of the rotor speed and the forward flight velocity. This velocity is time-varying because, as the rotor blade travels forward (in the same direction as the rotorcraft is flying), the relative velocity due to the flight of the drone is subtracted from the relative velocity due to the rotor rotation. As the blade travels backward (in the opposite direction to the rotorcraft flight), the opposite happens and the relative velocity increases. The relative velocity can thus be written as

$$v(t, s) = \omega s + v_f \sin(\omega t), \tag{11}$$

where s is the distance from the hub of the rotor ω is the angular velocity of the rotor and v_f is the forward velocity of the drone. Additionally we define the rotational velocity of the wing tip as

$$v_r = \omega s. \tag{12}$$

We computed the stability chart of the three-dimensional model by carrying out numerical simulations with the initial condition $\alpha_1(0) = 0.1$. We ran the simulations for 100 s and considered the system unstable if the tip rotation exceeded 0.1 at any point during the simulation, i.e., the system is considered unstable if

$$\exists t : \alpha_n(t) > 0.1. \tag{13}$$

The stability charts for different n values are shown in Figures 5, 6, 7. The blue region indicates the unstable region, while the yellow region indicates the stable region.

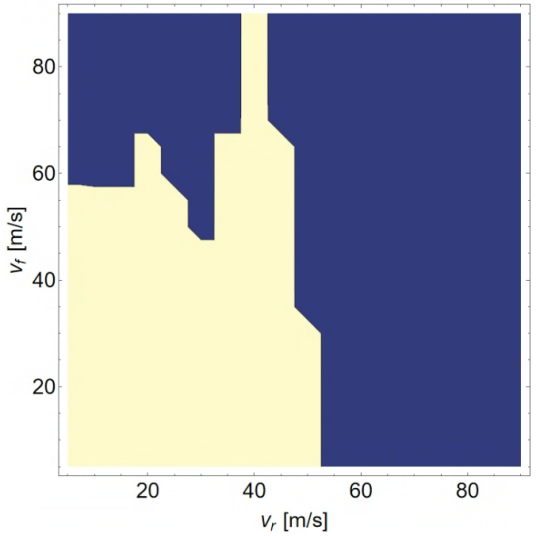

Figure 5. Stability chart for $n = 1$.

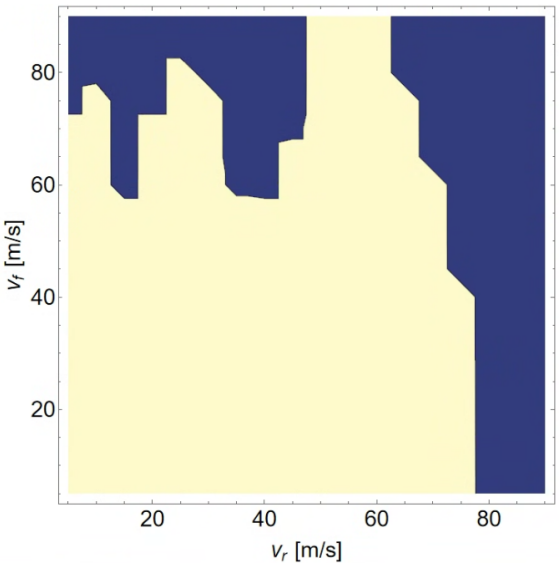

Figure 6. Stability chart for $n = 5$.

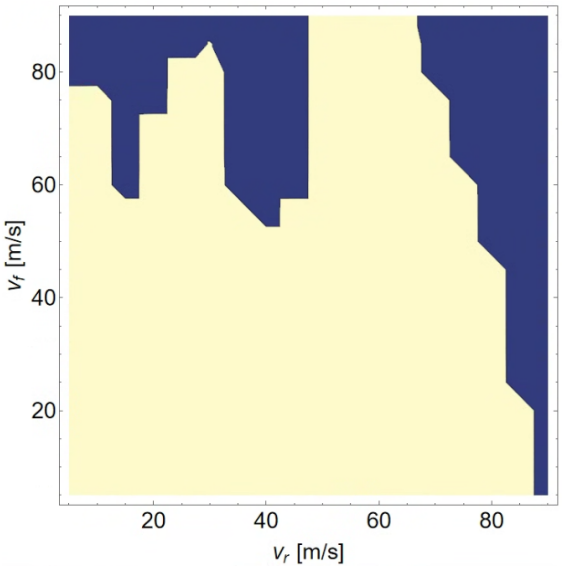

Figure 7. Stability chart for $n = 10$.

For a stationary drone, where the forward velocity $v_f = 0$, the critical velocity is 88 m/s as shown in the previous section. As the forward velocity v_f increases, the rotor will lose its stability at various v_f values depending on the tip velocity v_r. If $v_r < 50$ m/s, the stability loss occurs at $50 \leq v_f \leq 90$ m/s. However, these forward velocities are not attainable since the drone is not able to fly forward faster than the tip velocity. For $50 < v_r < 65$ m/s, the stability loss occurs at $v_f > 90$ m/s. Above $v_r = 65$ m/s, the stability boundary starts to decrease as v_r increases and reaches $v_f = 0$ m/s at the critical velocity $v_r = 88$ m/s. The stability charts corresponding to a lower number of wing segments have a similar shape but the unstable regions are larger.

4. FLUTTER SAFETY MARGIN

In this section, we define the flutter safety margin and compute it during a flight of the drone. The flutter safety margin is defined as the minimal increase in the relative wind velocity at the tip of the wing, which would result in flutter oscillations. This is defined mathematically as the distance between the point (v_f, v_r) and the stability boundary, i.e.,

$$\mathcal{S}(v_f, v_r) = \text{dist}((v_f, v_r), \mathcal{B}), \tag{14}$$

where $\mathcal{S}$ is the flutter safety margin, v_f is the forward velocity of the drone, v_r is the rotational velocity of the wing tip, and $\mathcal{B}$ is the stability boundary in the (v_f, v_r) plane.

To compute the flutter safety margin during the flight of the drone, we first measured the rotor speed corresponding to different forward flight velocities. The goal of the measurement was to determine the working range of a general drone propeller, not to validate the model. We carried out this measurement in the departmental wind tunnel. The drone was fixed inside the wind tunnel on a force measurement device so that we could measure the aerodynamic forces acting on the drone. We then set a constant wind velocity and increased the velocity of the drone rotors until the net force acting on the drone was zero. In this state, the lift of the rotors counteracts the aerodynamic drag and gravity. This means that the velocity of the drone rotors is the same as it would be during forward flight. The measurement setup is shown in Figure 8.

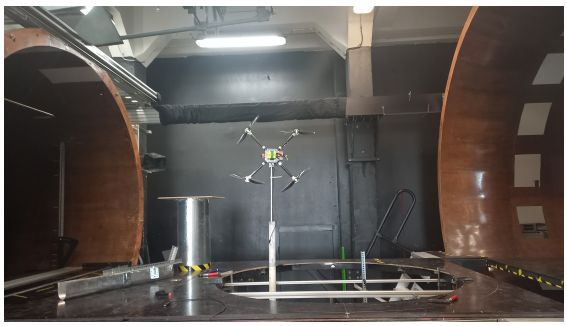

Figure 8. The measurement of the drone rotor velocities in the wind tunnel.

The result of the measurement is shown in Figure 9 and Table 2, where f denotes the rotational velocity of the propeller in revolutions per minute.

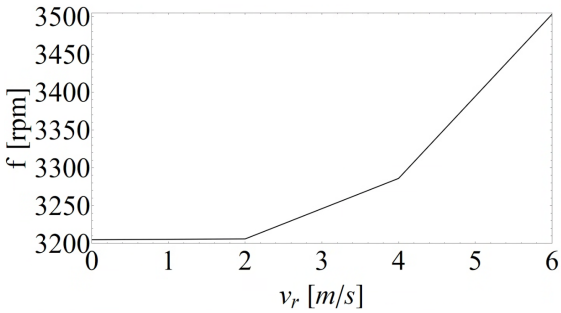

Figure 9. The rpm of the drone rotor at different forward flight velocities

v [m/s]	n [rpm]
0	3205
2	3206
4	3286
6	3503

Table 2. The velocity of the drone rotor at different forward flight velocities

As the forward velocity of the drone increases, the rotor velocity also increases, which becomes more apparent at higher forward velocities. Note that these rotor velocities result in a rotor tip velocity above the critical velocity for the two-dimensional reduced-order model (which is 52 m/s). Thus, this measurement confirms that the three-dimensional reduced-order model is indeed more accurate than the two-dimensional one.

We show the drone's forward flight velocities

and the corresponding rotor tip velocities on the stability chart in Figure 10 with a black line.

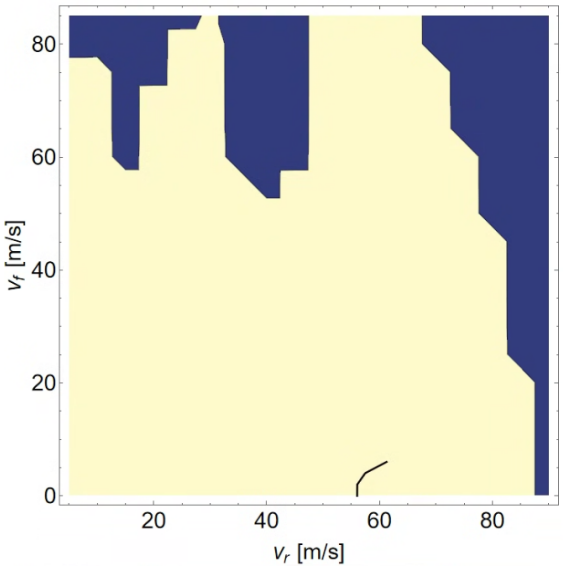

Figure 10. The rotor tip velocities and their corresponding forward flight velocities shown on the stability chart.

The drone stays well away from the stability boundary during forward flight, so flutter does not occur. This again confirms that the three-dimensional model results in more accurate results than the two-dimensional model since the latter predicts that the drone is in the unstable regime during flight. The flutter safety margin is shown in Table 3. As the drone accelerates, the flutter safety margin decreases, but remains above $20m/s$, so there is no risk of flutter.

$v\ [m/s]$	$n\ [rpm]$	$\mathcal{S}\ [m/s]$
0	3205	25.95
2	3206	25.93
4	3286	24.53
6	3503	20.74

Table 3. The flutter safety margin during forward flight

5. SUMMARY

In this paper, we develop a three-dimensional reduced-order model for wing flutter. This model is built by chaining multiple two-dimensional reduced-order models together using linear springs. As a result, each wing segment in the three-dimensional model has a pitch and a plunge degree of freedom, but these are influenced by the motion of the neighboring wing segments.

First, we computed the critical velocity (i.e., the smallest velocity at which flutter is present) for the three-dimensional model as a function of the number of wing segments. We found that the use of multiple wing segments results in an increase in the critical velocity. As the number of wing segments increases, the critical velocity converges to a fixed value and does not increase indefinitely. We also concluded that the use of a linear velocity distribution along the wing results in an even greater critical velocity.

Next, we computed stability charts using the three-dimensional model for various n values and found that increasing the number of wing segments results in the enlargement of the stable region. Based on the stability chart, we defined a flutter safety margin as the distance from the stability boundary. To compute the flutter safety margin during flight, we performed wind tunnel measurements to obtain the rotor tip velocity for different forward flight velocities. Based on the measurement results, we computed the flutter safety margin during forward flight and found that it decreases as the drone accelerates, but never approaches zero, so flutter does not develop during the flight of the drone.

ACKNOWLEDGEMENTS

This work has been supported by the Hungarian National Research, Development and Innovation Fund under contract NKFI K137726.
The research reported in this paper is part of project no. TKP-6-6/PALY-2021 has been implemented with the support provided by the Ministry of Culture and Innovation of Hungary from the National Research, Development and Innovation Fund, financed under the TKP2021-NVA funding scheme. The project supported by the Doctoral Excellence Fellowship Programme (DCEP) is funded by the National Research Development and Innovation Fund of the Ministry of Culture and Innovation and the Budapest University of Technology and Economics.

REFERENCES

[1] Bisplinghoff, R. L., Ashley, H., and Halfman, R. L., 2013, *Aeroelasticity*, Courier Corporation.

[2] Dowell, E. H., 2015, *A Modern Course in Aeroelasticity*, Springer.

[3] Fung, Y. C., 2008, *An Introduction to the Theory of Aeroelasticity*, Courier Dover Publications.

[4] Dowell, E. H., Curtiss, H. C., Scanlan, R. H., and Sisto, F., 1989, *A modern course in aeroelasticity*, Vol. 3, Springer.

[5] Harish, A., "Why the Tacoma Narrows Bridge Collapsed: An Engineering Analysis", `https://www.simscale.com/blog/2018/07/tacoma-narrows-bridge-collapse/`, accessed: 2020-07-10.

[6] "Tacoma Narrows Bridge (1940)", `https://en.wikipedia.org/wiki/Tacoma_Narrows_Bridge_(1940)`, accessed: 2020-07-10.

[7] Meshki, M. M., Nobari, A. S., and Sadr, M. H., 2020, "A study on nonlinear, parametric aeroelastic energy harvesters under oscillatory airflow", *Journal of Vibration and Control*, pp. 1–11.

[8] Lelkes, J., Horváth, D. A., Lendvai, B., Farkas, B., Bak, B. D., and Kalmár-Nagy, T., 2023, "Data-driven aerodynamic models for aeroelastic simulations", *Journal of Sound and Vibration*, Vol. 593, p. 117847, URL `https://www.sciencedirect.com/science/article/pii/S0022460X23002961`.

[9] Abdelkefi, A., Vasconcellos, R., Nayfeh, A. H., and Hajj, M. R., 2013, "An analytical and experimental investigation into limit-cycle oscillations of an aeroelastic system", *Nonlinear Dynamics*, Vol. 71 (1-2), pp. 159–173.

[10] Theodorsen, T., 1935, "General theory of aerodynamic instability and the mechanism of flutter", *NACA Technical Report*, (496).

[11] Horváth, D. A., 2021, "Investigation of a reduced mathematical model of a rotor blade", Bachelor Thesis, Budapest University of Technology and Economics.